Available online at www.sciencedirect.com
SCIENCE DIRECT®
Control Engineering Practice 14 (2006) 1035–1043
CONTROL ENGINEERING PRACTICE
www.elsevier.com/locate/conengprac

A contact detection algorithm of the z-axis of a wire bonder

Jung-Han Kim*, Hee-Jae Park

School of Mechanical Design and Automation Engineering, Seoul National University of Technology, 172 Gongneung-dong, Nowon-ku, Seoul 139-743, Korea

Received 26 June 2004; accepted 19 June 2005
Available online 27 July 2005

Abstract

A new design of contact detection algorithm is proposed for the z-axis of a wire bonder that interconnects between pads and leads in semiconductor manufacturing processes. The proposed test parameter for contact detection is statistically designed using the relation between Kalman filter propagations, and it has a simple process for defining probability of false alarm. Fast and stable contact detection of the z-axis is extremely important for maintaining proper quality in the fine pitch gold wire bonding process, which has a small pad size of below 70 μm. Experimental results are presented to demonstrate the advantages of the proposed algorithm.

Keywords: Detection algorithms; Stochastic parameters; Detecting elements; Modeling errors; Kalman filters; Filtering problem

1. Introduction

Recently, the number of interconnections in typical semiconductor assembly process has increased by approximately three times or more, leading to smaller pads and balls in wire bonding process. Smaller pad size and finer pitch require various new techniques such as faster and more stable contact detection, precise force control, and smooth control mode changes in transient areas. These techniques have changed the function and structure of the wire bonder and necessitate a deeper understanding of the wire bonding process (Rooney, Nager, Geiger, & Shanguan, 2005).

When the capillary of the z-axis contacts on a pad, it impacts with a free air ball (FAB), and some part of FAB forms an inter-metallic boundary. The FAB is made by a high-voltage spark to the end of a gold wire. After contact on the pad surface, the FAB is transformed into a squashed bonded ball by ultrasonic energy and bonding force. At that moment, various factors affect the squashed ball qualities such as bonding strength and size variation. These factors include the contact detection time, mode change time to force control after detection, impacting force by the bond head inertia, z-axis force by motor current, FAB size and so on. These factors are more critical to small ball formation in fine pitch pad bonding. Among them, the contact detection time and the force control of the z-axis in fine pitch are of critical importance (Leonhardt, 1997). To obtain a uniform squashed ball size and bonding quality with consistency, it is necessary to obtain accurate contact detection information of the z-axis.

The surface detection problem in wire bonding process has common points with the disturbance detection and failure detection problems in the Kalman filter application. The detection of disturbances is closely related to model changes and parameter estimation such as the target tracking system. For example, in the airplane tracking problem, if a pilot accelerates or turns an airplane, the system model is changed. In this case, to change the system model in the filtering algorithm, it should be found out as soon as possible in noisy measurement. Blair developed two stage estimators and used the bias vector to detect change in

*Corresponding author. Tel.: +82 2 970 6397; fax: +82 2 974 8270.
E-mail address: hankim@snut.ac.kr (J.-H. Kim).

0967-0661/$ - see front matter © 2005 Elsevier Ltd. All rights reserved.
doi:10.1016/j.conengprac.2005.06.004

the system model (Blair, 1993). Failure detection using a generalized likelihood-ratio test was also developed for a multiple model change (Willsky & Jones, 1976). Mangoubi summarized the techniques of failure detection (Mangoubi, 1998).

These related works can be divided into three general categories, parameter estimation, parameter change detection, and multiple model changes. Researchers in the field of radar applications have been actively developing solutions to these kinds of problems. For example, Bogler used the residual of the Kalman filter to check its optimality (Bogler, 1987). These problems share a common issue—how to detect the change of models.

The work in this paper is related to the detection of system change, but the detection methods from target tracking systems are designed for tracking an airplane, and in addition, they are too complex to be installed in commercial control systems such as wire bonder machines. The work in this paper has a distinction point of using very simple and effective test parameter q_k that can be installed in the conventional DSP motion control hardware. The new test parameter q_k is designed for real time contact detection of the z-axis of a wire bonder machine.

In this paper, a novel contact detection algorithm for a wire bonder is suggested. The suggested algorithm is designed based on a stochastic approach and it can be easily carried out using the parameters of the discrete Kalman filter. The following sections describe the design procedure of the new algorithm and application results of a fine pitch wire bonding process.

2. Gold wire bonding process

The gold wire bonding process is characterized as a thermosonic process. This means that heat, ultrasonic, and force are used to execute the bond (Lui, Chao, & Wang, 2004). All of these parameters are related to the z-axis control and the capillary contact condition. Fig. 1 shows a sequence of a typical gold wire bonding process. There are two contacts in the formation of one wire. Generally, the first contact of the capillary is executed on the pad of a fabricated chip, and the second contact is on the lead of a leadframe. After FAB formation by electronic flame off (EFO), a capillary with a gold ball rapidly descends to the search level, and then proceeds to the pad surface with a constant speed until it contacts the pad (Fig. 1(a)). Every pad and lead has a slightly different contact level, because there is always variation of epoxy thickness and mechanical clamping status.

After the first contact detection, the capillary is forced down by a bonding force with ultra-sonic energy (Fig. 1(b)). After the first bonding process, the capillary moves to the loop top position through a kink motion

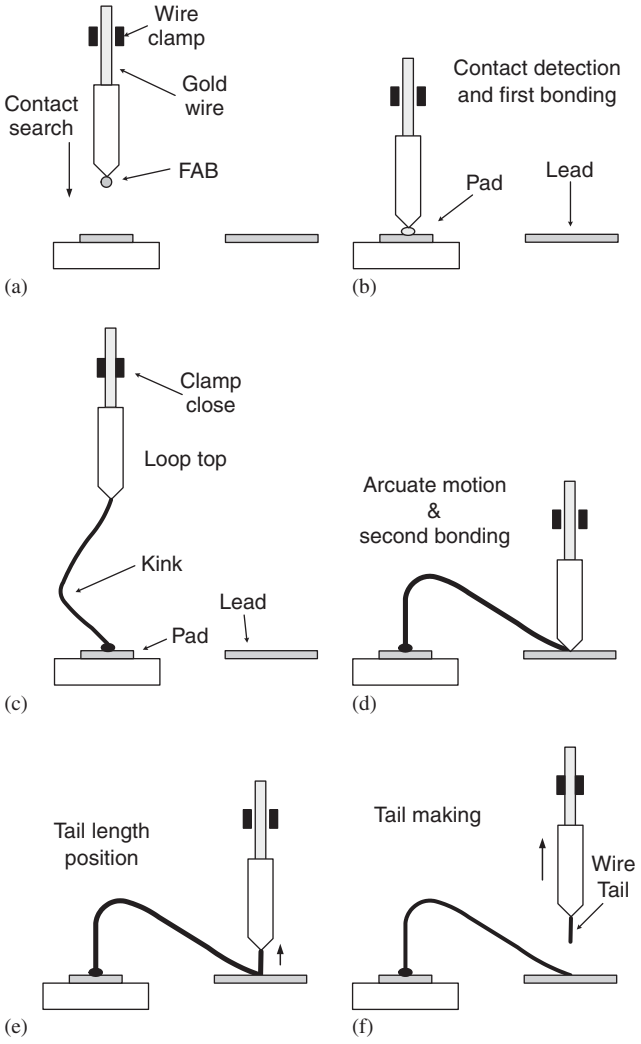

Fig. 1. Gold wire bonding sequence: (a) capillary descends with gold ball, (b) contact and make first bonding, (c) make kink and proceed to loop top, (d) arcuate motion and second bonding, (e) proceed to tail length position, (f) close clamp and make tail.

(Fig. 1(c)). It subsequently travels to the second search position with arcuate motion and finds the second contact, at which time it makes the second bonding (Fig. 1(d)). After the second bonding, the capillary travels to the tail height with an opened wire clamp (Fig. 1(e)) and then moves to the EFO level with a closed wire clamp (Fig. 1(f)).

There are three critical disturbances related to contact detection in the wire bonding process described above. The first disturbance is the electric current limitation of the z-axis for preventing chips from damage during capillary contact. Fig. 2 illustrates a capillary descending for contact. During the z-axis search for contact, the maximum current of the z-axis should be limited below the bonding force, which has a typical value of 5–20 g for a pad, because there is a small time delay between the moment of real contact occurred and the moment it

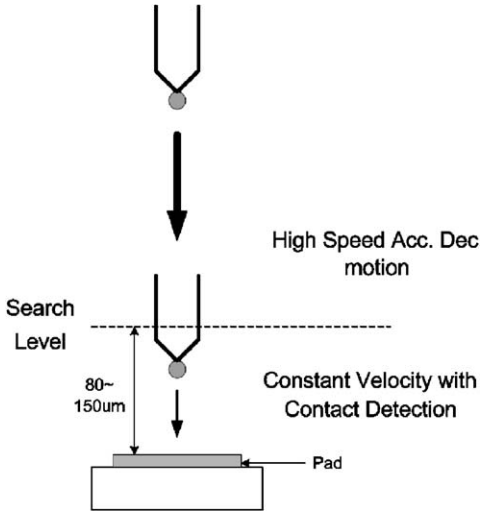

Fig. 2. Capillary descends for contact detection.

Fig. 3. Front view of the head of wire bonder.

recognized. If the current of z-axis is unlimited, at the contact moment the z-axis will push down the FAB by big control current until the contact recognized, and finally it produces a big over-sized squashed bonded ball. The limited current makes it difficult to control the z-axis with a constant velocity, because the limited value is so small (5–20 g) for controlling the z-axis in the presence of disturbances from the spring hinge, cable tension, friction, vibration and so on.

Basically the contact detection algorithms of wire bonders use the z-axis velocity information as a most important factor. During the contact searching mode, the z-axis moves downward in a constant velocity control mode. At that time, if a certain disturbance causes an excessive velocity perturbation of the z-axis before contact, the contact detection algorithm will make a false detection in the empty space, and consequently the control mode of the z-axis is changed into force control mode before real contact being occurred. After that finally the z-axis crushes into the silicon pad. For making a fine pitch wire bonding, the bonding force should be reduced significantly, and as such the velocity information and stable contact detection are critically important.

Another disturbance arises from mechanical structural vibration. The z-axis descends with very high acceleration and deceleration until reaching the search level, which is generally 80–150 μm above the contact level. A state-of-the-art wire bonder system has a maximum acceleration of $100G$ for the z-axis, and consequently a large amount of excitation force for the mechanical structural vibration remains after deceleration. This vibration is a significant obstacle to obtaining an accurate estimation of the z-axis velocity. Therefore, several IIR digital filters should be used for reduction of structural vibration noise in addition to the state estimator. The contact detection algorithm should have immunity from this vibration noise. Fig. 3 shows the front view of the wire bonding head, which has a long cantilever-type ultrasonic horn. The capillary is attached at the end of the ultrasonic horn.

The third disturbance for contact detection arises from the gold wire feeding system. This system has several air blowers and a tensioner that causes wire vibration during bonding. The gold wire vibration affects the z-axis velocity control during the contact search. The wire tensioner also affects the movement of the z-axis when the wire clamp is open.

The aforementioned disturbances make it difficult to detect contact with stable detection time. This in turn affects the ball squash variation, which is tightly controlled, especially for the fine pitch wire bonding. The following sections describe the design of the velocity estimator and the contact detection algorithm based on a statistical approach.

3. Design of the optimal velocity estimator for the z-axis

For fine pitch wire bonding, the search velocity should be slower than that employed in the case of a normal size pad, because the impact force of the z-axis must be reduced. Therefore, the number of encoder pulses per control interrupt is decreased. In this case, the velocity estimator becomes more important, because the velocity information is used for one of the inputs of the contact detection algorithm. A z-axis moving with constant velocity can be modeled by the following equations:

$$\mathbf{x}_{k+1} = \mathbf{F}_k \mathbf{x}_k + \mathbf{b}_k u_k + \mathbf{G}_k \mathbf{w}_k, \tag{1}$$

$$z_k = \mathbf{h}_k \mathbf{x}_k + v_k, \tag{2}$$

$$\mathbf{x}_k = \begin{bmatrix} x_p \\ x_v \end{bmatrix}, \quad \mathbf{F}_x = \begin{bmatrix} 1 & \Delta t \\ 0 & 1 \end{bmatrix}, \quad \mathbf{h}_k^{\mathrm{T}} = \begin{bmatrix} 1 \\ 0 \end{bmatrix},$$
$$\mathbf{b}_k = \begin{bmatrix} \frac{1}{2}\Delta t^2 \\ \Delta t \end{bmatrix}, \quad \mathbf{G}_k = \begin{bmatrix} 1 & 0 \\ 0 & 1 \end{bmatrix}, \tag{3}$$

where Δt is the sampling time, $\mathbf{G}_k$ is the process noise input matrix and u_k is the acceleration input of the z-axis. The observation z_k is corrupted by noise v_k, which has a variance of R_k. To obtain finer resolution from an industrial encoder, which normally has 4–20 μm grating pitch resolution, an electrical subdividing circuit is required. The phase subdividing circuit is composed of several analog components and A/D converters, and as such the output of the subdividing circuit contains perturbation largely come from electrical noises. Electrical noises mainly come from several sources such as the thermal noise, the shot noise, the burst noise and etc. It is known that these intrinsic noises can be modeled as a Gaussian that has a variance of R_k (Ott, 1989). The process noise $\mathbf{w}_k$ is also assumed as a Gaussian. The discrete Kalman filter equations are summarized in Eqs. (4)–(8) (Chui & Chen, 1991).

Time update:

$$\hat{\mathbf{x}}_{k/k-1} = \mathbf{F}_{k-1}\hat{\mathbf{x}}_{k-1/k-1} + \mathbf{b}_k u_k, \tag{4}$$

$$\mathbf{P}_{k/k-1} = \mathbf{F}_{k-1}\mathbf{P}_{k-1/k-1}\mathbf{F}_{k-1}^{\mathrm{T}} + \mathbf{G}_{k-1}Q_{k-1}\mathbf{G}_{k-1}^{\mathrm{T}}. \tag{5}$$

Measurement update:

$$\mathbf{K}_k = \mathbf{P}_{k/k-1}\mathbf{h}_k^{\mathrm{T}}(\mathbf{h}_k\mathbf{P}_{k/k-1}\mathbf{h}_k^{\mathrm{T}} + R_k)^{-1}, \tag{6}$$

$$\hat{\mathbf{x}}_{k/k} = \hat{\mathbf{x}}_{k/k-1} + \mathbf{K}_k(z_k - \mathbf{h}_k\hat{\mathbf{x}}_{k/k-1}), \tag{7}$$

$$\mathbf{P}_{k/k} = \mathbf{P}_{k/k-1} - \mathbf{P}_{k/k-1}\mathbf{h}_k^{\mathrm{T}}(\mathbf{h}_k\mathbf{P}_{k/k-1}\mathbf{h}_k^{\mathrm{T}} + R_k)^{-1}\mathbf{h}_k\mathbf{P}_{k/k-1}. \tag{8}$$

The key factor in designing the optimal estimator of Eqs. (4)–(8) is the determination of R_k and Q_k. The variance R_k can be determined by measuring the output of the subdivided encoder signal when the z-axis is tied to a stable block when the x–y stage is regulating control status. If there is a slow frequency drift, it can also be considered. The Q_k value has to be determined by a real bonding experiment in order to consider all the disturbances described in Section 2. The velocity estimator may be used both in the searching area before contact and in the entire wire bonding process. If the estimated velocity information is used only in the contact searching area, the variance parameter R_k and Q_k can be specially optimized for the searching motion.

4. Design of the contact detection algorithm

Below the search level, the bonding tip descends with constant velocity. Within this constant velocity moving area, the error covariance propagation (Eqs. (5) and (8)) shows an oscillation phenomenon, as in Fig. 4 (Kim & Oh, 2000). The difference between the two update processes (the second term of RHP of Eq. (8)) means the reduction of uncertainty by reflecting current measurement, therefore, if the measurement noise has a big covariance R, then the quantity of reduction will be small. When the bonding tip is descending with constant speed, which can be modeled as a constant velocity model, the error covariance difference between the two update processes is statistically equal to the length of the vertical line drawn in each step of Fig. 4.

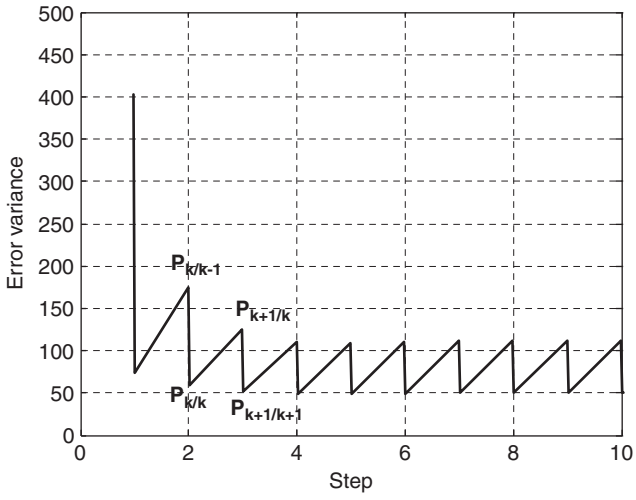

Fig. 4. Error covariance propagation of Kalman filter.

The difference between the two update processes (the vertical line drawn in each step) shows a reduction of error covariance by measurement and filter proceeding, and can be used as a reference for determining whether the velocity perturbation arises from noise or from real contact. If the difference can be described as a certain parameter that includes real measurement, it is possible to verify in real time whether the bonding tip achieves contact. In other words, the normalized vertical line of Fig. 4 can be used as a reference for the decision of the contact detection at every sampling moment. Theorem 1 connects the measure of expectation to the real measurement space.

Theorem 1. *The difference between the two-covariance matrices can be described as an expectation function of innovations process and optimal gain K.*

$$\mathbf{P}_{k/k-1} - \mathbf{P}_{k/k} = E[\mathbf{K}_k\mathbf{v}_k\mathbf{v}_k^{\mathrm{T}}\mathbf{K}_k^{\mathrm{T}}], \tag{9}$$

where innovations $\mathbf{v}_k = \mathbf{z}_k - \mathbf{h}_k\hat{\mathbf{x}}_{k/k-1}$.

Proof. Given in Appendix A.

Theorem 1 describes the relation between the difference of the two covariance matrixes and real measurement data. The right-hand side of Eq. (9) can be

calculated from the innovation processes that include the real measurement data at each step. By using the left-hand side of the pre-determined statistical error covariance, it is possible to determine whether the velocity of the bonding tip contacts the pad. For further development, a process c_i is defined as

$$c_i = \mathbf{h}_i \mathbf{K} \mathbf{v}_i. \tag{10}$$

The process c_i has zero mean and normal distribution because $\mathbf{v}_i$ is an innovation process (Kailath, 1968). Therefore, the square of process c_i has a chi-square distribution. In order to verify the chi-square distribution in real time, Pearson's test statistic is introduced (Harvey, 1992)

$$q_k = \sum_{k-n}^{k} \frac{(c_i - E[c_i])^2}{\mathrm{var}(c_i)} \tag{11}$$

where n denotes the size of the sample window. The variance of c_i is

$$E[(c_i - \bar{c}_i)(c_i - \bar{c}_i)^{\mathrm{T}}] = E[c_i c_i^{\mathrm{T}}] = E[\mathbf{h}_i \mathbf{K}_i \mathbf{v}_i \mathbf{v}_i^{\mathrm{T}} \mathbf{K}_i^{\mathrm{T}} \mathbf{h}_i^{\mathrm{T}}]. \tag{12}$$

By Theorem 1, the variance of c_i can be represented by the difference between $\mathbf{P}_{i/i-1}$ and $\mathbf{P}_{i/i}$. In the denominator of Eq. (11), if only the real measurable state is considered, the complete form of Eq. (11) using theorem 1 is

$$q_k = \sum_{k-n}^{k} \frac{(c_i)^2}{\mathbf{h}_i(\mathbf{P}_{i/i-1} - \mathbf{P}_{i/i})\mathbf{h}_i^{\mathrm{T}}} = \sum_{k-n}^{k} \frac{(\mathbf{h}_i \mathbf{K}_i \mathbf{v}_i \mathbf{v}_i^{\mathrm{T}} \mathbf{K}_i^{\mathrm{T}} \mathbf{h}_i^{\mathrm{T}})}{\mathbf{h}_i(\mathbf{P}_{i/i-1} - \mathbf{P}_{i/i})\mathbf{h}_i^{\mathrm{T}}}. \tag{13}$$

There is not much additional computational cost to calculate the test parameter q_k, because all the matrixes used in Eq. (13) are also necessary for discrete Kalman filter updating. The chi-square degree of freedom $(n-1)$ is determined appropriately by the sampling frequency and the endurable detection delay.

The physical meaning of the test parameter q_k is a statistical information parameter concerning the change of velocity that results from contact of the bonding tip. By the normalized parameter q_k, it is possible to use the standard table of the chi-square to determine the threshold of alarm level and the probability of false alarms (PFA). For example, when the window size is 6 (degree-of-freedom is 5) and the sampling frequency is 4 kHz, 95% confidence is obtained if the threshold is set at 11.070 and the detection delay is approximately 1.5 ms. In this manner, the PFA of the test parameter q_k is determined at a certain risk. In a real manufacturing process, 95% confidence is insufficient for wire bonding, and therefore in this paper a contact test function $Q(k)$ composed of a series of Pearson's test parameters is suggested. Consider a unit step function defined as

$$1(k) = \begin{cases} 1, & k \geqslant 0, \\ 0, & k < 0. \end{cases} \tag{14}$$

Table 1
Example table of PFA when $n = 3$

Confidential level α_k			Probability of false alarm
k (%)	$k-1$ (%)	$k-2$ (%)	Part per million (ppm)
3	3	2	18
3	2	1	6
2	2	2	8
2	2	1	4

The final contact test function $Q(k)$ is suggested as

$$Q(k) = 1(q_k - \alpha_k) \times 1(q_{k-1} - \alpha_{k-1}) \times 1(q_{k-2} - \alpha_{k-2}) \times \cdots \times 1(q_{k-n} - \alpha_{k-n}), \tag{15}$$

where α_k is a certain threshold level from the standard chi-square table. n is the number of q_k that will be considered. For example, when three samples of q_k are used, if the confidence parameter α_k is set at 2%, 2%, and 1% for k, $k-1$, $k-2$ steps, respectively, then the final PFA is about 4 ppm, which is a level that is equal to a 6σ process. The test function $Q(k)$ can be easily extended to use more than three samples by increasing the parameter n when the sampling frequency is higher (Table 1).

5. Experiment results

Fig. 5 presents the block diagram of the experimental bonding system. The resolution of the encoder is about 0.438 μm and the sampling frequency is 4 kHz. Three of the IIR notch filters are used for reducing the vibration noise, and the velocity signal is filtered by the Kalman filter. The velocity controller then controls the z-axis with a constant velocity in the contact searching area. At every measurement step, the Kalman filter gives parameters $\mathbf{K}_k$, $\mathbf{P}_{k/k}$, and $\mathbf{P}_{k/k-1}$ for the calculation of q_k. The q_k is used for calculating the test function $Q(k)$ and finally it is compared with the standard chi-square table for determination of contact (the degree-of-freedom of q_k is 5).

As described in Section 2, the ultrasonic horn has a long structure, and hence the raw velocity information is corrupted with large vibration noise in the searching area, as illustrated in Fig. 6.

The thick line of Fig. 6 shows the raw velocity information made by simple differentiation of the encoder signal between control interrupts. For reducing this vibration noise, several IIR digital filters and a Kalman filter should be used. Fig. 7 shows a bode plot of one of three IIR notch filters that has a blocking frequency of 750 Hz (one of the mechanical resonances). These digital filters make additional phase delay in the

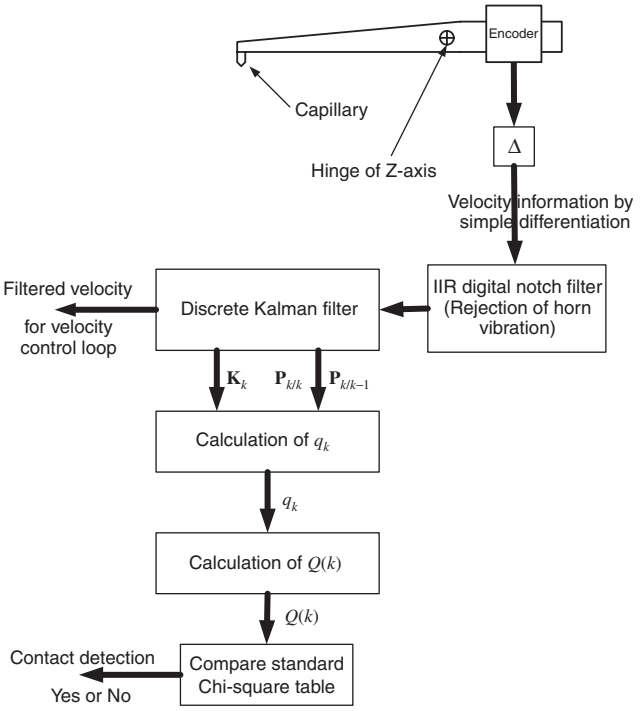

Fig. 5. Block diagram of the experimental system.

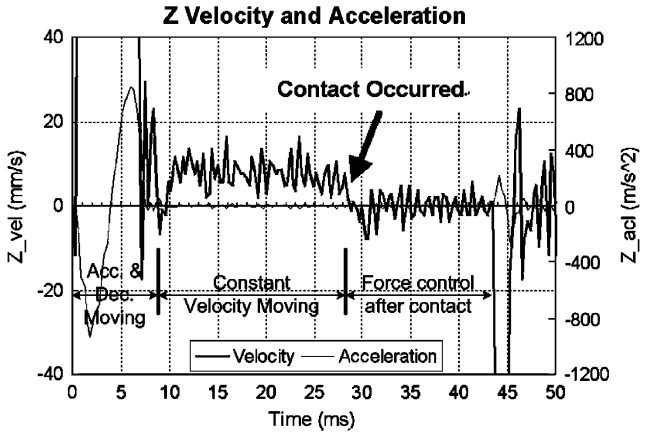

Fig. 6. z velocity and acceleration when the capillary contacts a pad.

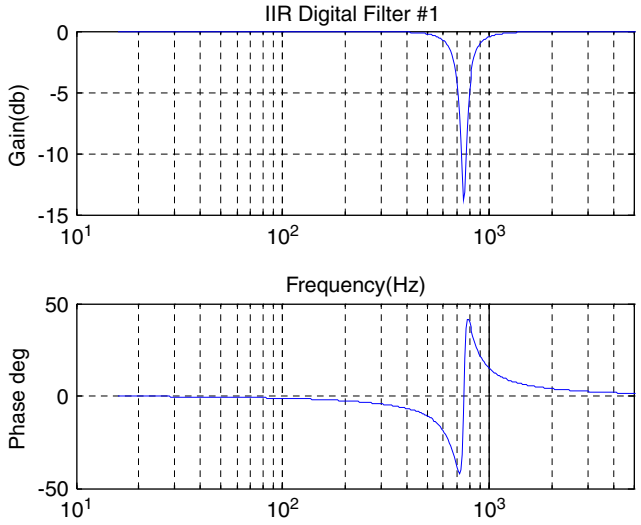

Fig. 7. Bode plot of the digital IIR notch filter for vibration rejection.

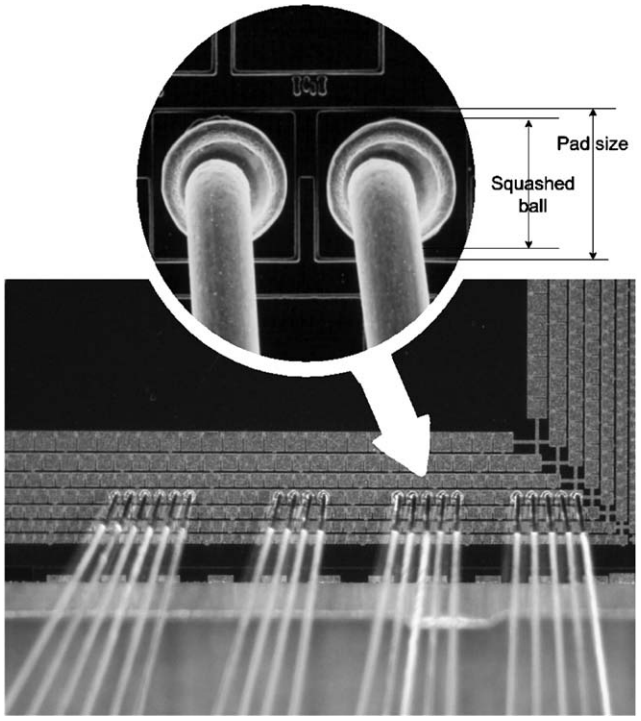

Fig. 8. Pad side of fine pitch gold wire bonding.

control loop which makes more tracking errors, therefore, the number of digital filters in the control loop should be minimized.

Semiconductor devices, each having 126-pad and 208-pad (both have 70 μm pad pitch), were monitored in experiments. The experiment data were gathered in a real wire bonding production line. Fig. 8 shows a magnified picture of the pad side of the wire bonding process.

Fig. 9 shows a captured signal when the capillary contacts a pad (window size $n = 3$, PFA = 8 ppm). For the experiments, a four-channel D/A converter is attached to the DSP board that controls the z-axis of the wire bonder. Using the four-channel D/A, the parameters inside the DSP can be easily measured and captured in real time. Fig. 9 shows the four parameters inside the DSP related with contact detection. Channel 1 shows the velocity output filtered by the Kalman filter, which is explained in Section 3 and illustrated in Fig. 5. The trigger position is the moment that the z-axis passes through the search level, as illustrated in Fig. 2. Below the search level, the z-axis control mode is changed to the constant velocity mode for contact detection.

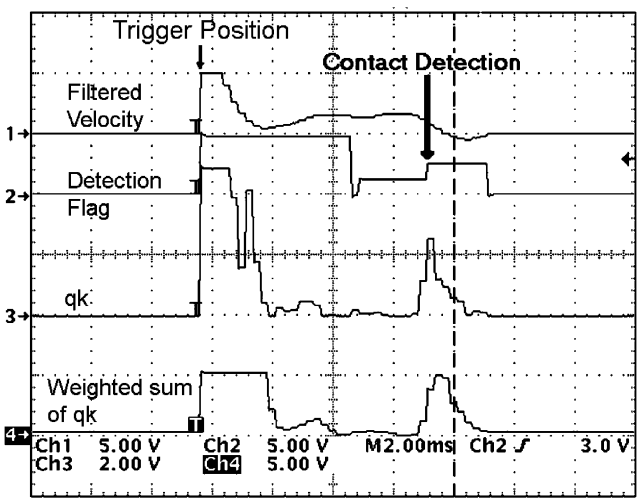

Fig. 9. Contact detection parameters: Channel 1: velocity information from Kalman filter, Channel 2: detection status of proposed detection algorithm, Channel 3: test parameter q_k, Channel 4: weighted summation of the q_k.

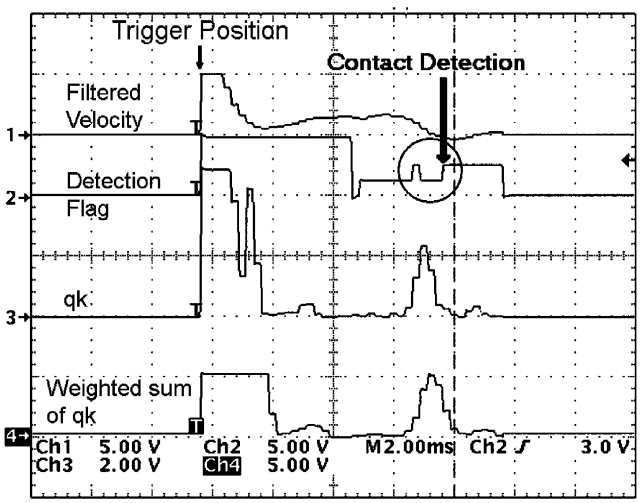

Fig. 10. Contact detection parameters: Channel 1: velocity information from Kalman filter, Channel 2: detection status by the constant threshold method, Channel 3: test parameter q_k, Channel 4: weighted summation of the q_k.

Channel 2 shows a detection status flag by the proposed method. The signal shows ready-to-detect status when it maintains about 1 V. Channel 3 shows the test parameter q_k, which is defined in Eq. (13). The detection decision value (α_k) for this experiment is scaled as about 1.2 V (2% error for each q_k). Finally, Channel 4 is a test parameter for checking the algorithm (weighted summation of the q_k).

The detection result of the test function q_k (channel 3) displays a very fast detection response and a stable signal in a real wire bonding process. First of all, the statistical design of $Q(k)$ provides systematic guidelines to manage the risk of false detection from the viewpoint of a semiconductor assembly process, especially to handle MTBA (mean time between assist) in a gold wire bonding process.

To express the advantage of the suggested detection method numerically, the same test function as Eq. (15), except for the use of a constant threshold and filtered velocity instead of q_k, is compared with the suggested method. If the filtered velocity of the z-axis goes below a certain threshold, then it outputs a contact detection flag in the first cell of Eq. (15). In most cases, the velocity information is a major factor for detection, and detection algorithms usually have the serial structure like Eq. (15) for improving reliability. It should be noted that many kinds of current wire bonder machines use similar detection methods. By the experiment, it was found that the method using a constant threshold occasionally makes delayed outputs. Fig. 10 shows a captured data of delayed detection timing of the constant threshold method.

Channel 2 of Fig. 10 shows the delayed time by the constant threshold method. The contact detection flag returned to the ready-to-detect status during 0.7 ms before the detection was finally recognized. This means that a wrong detection interrupted Eq. (15) by noise in the detection sequence. During this delayed detection time, the capillary tip is descending further and exerting more force on the gold ball on the pad, and consequently the squashed ball size becomes bigger when there is delayed detection time. The method using a constant threshold cannot efficiently reject the disturbance from a noisy velocity signal, because of the structural limitation from the simple constant threshold.

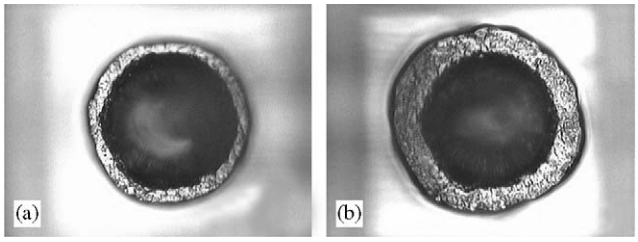

Fig. 11. Magnification of the bonded balls on pads: (a) normal bonded ball, (b) over-sized bonded ball.

Meanwhile, Channel 3 of the suggested algorithm (Fig. 10) shows stable detection characteristics of q_k. Fig. 10 clearly shows that the proposed detection method can reject this perturbation efficiently under the same conditions.

Fig. 11 shows two pictures of bonded balls on pads. There are several factors those make the over-sized bonded ball, such as delayed contact detection, over-pressed in the force control mode, excess ultrasonic power and etc. The delayed detection is one of the most important factors that produce such big-sized ball in silicon pad.

Table 2
Experimental results of the detection time

	Constant threshold		Proposed detection algorithm	
	126 Pads	208 Pads	126 Pads	208 Pads
Mean time $\bar{t}_d$	3.23 ms	3.32 ms	3.04 ms	3.07 ms
Standard deviation σ	0.1233	0.1344	0.0615	0.0781
Average	$\bar{t}_d = 3.28$ ms, $\sigma = 0.1289$		$\bar{t}_d = 3.06$ ms, $\sigma = 0.0698$	

For three chips of a 126-pad device (378 wires) and two chips of a 208-pad device (416 wires), the detection times were measured in a real production line of a wire bonding process. For every contact moment of 794 wires, the detection times by both methods are measured. The reference time line is the moment that the tip of the capillary passes through an area 1 milli-in above the contact level. Table 2 provides a summary of the experimental results of the two kinds of devices.

The detection time in Table 2 means the time between the reference time line and the acknowledged moment of contact detection. The 208-pad device has a softer substrate, and hence longer time is needed to detect the surface in both algorithms. For both devices, the proposed algorithm shows faster detection time and more stable signal characteristics, which is necessary in fine pitch gold wire bonding. Low standard deviation indicates stable performance of the detection algorithm, and this is very important for stabilizing the bonding strength and quality in the wire bonding process. The standard deviation of the proposed algorithm is nearly half of that by the constant threshold method. Larger standard deviation means that the delayed detection shown in Fig. 10 occurs with much higher frequency.

The popular reference for the cycle time in wire bonding is the entire bonding time of 2 mm distance. Recently, brand-new wire bonders have less than 65 ms cycle time. If there exists detection delay phenomenon, it affects the cycle time about 0.1–0.4%, but the delayed detection makes big difference in bonding quality and consistency of the product.

6. Conclusions

In order to facilitate finer pitch wire bonding, the contact time must be controlled more tightly. Variation of the detection time results in variation of the squashed ball size and unstable bonding quality. The proposed detection method shows more stable and faster detection time than that of the constant threshold detection method.

At every stage of a semiconductor manufacturing process, there is a certain range of variation of the characteristics of an individual device, and consequently the statistical approach of managing the output quality lends more stable quality in the final products of mass production processes. The statistical approach of the suggested algorithm is very helpful to build a stable process in assembly production lines.

In this paper, a new contact detection algorithm for a wire bonder based on statistics is suggested and tested. The experiments show that the proposed contact detection algorithm affords faster detection time and stable performance, which are essential to control the small ball in fine pitch gold wire bonding.

Appendix: Proof of Theorem 1

Define,

$$\tilde{\mathbf{x}}_{k/k} \equiv \hat{\mathbf{x}}_{k/k} - \mathbf{x}_k, \tag{16}$$

$$\tilde{\mathbf{x}}_{k/k-1} \equiv \hat{\mathbf{x}}_{k/k-1} - \mathbf{x}_k. \tag{17}$$

The $\mathbf{x}_k$ is the system state that is defined in (3), and the innovations process is

$$\mathbf{v}_i = \mathbf{z}_i - \mathbf{h}_i \hat{\mathbf{x}}_{i/i-1}, \tag{18}$$

where v_k is the measurement noise term define in Eq. (2).

$$\begin{aligned} &E[(\hat{\mathbf{x}}_{k/k-1} - \hat{\mathbf{x}}_{k/k})(\hat{\mathbf{x}}_{k/k-1} - \hat{\mathbf{x}}_{k/k})^{\mathrm{T}}] \\ &\quad = E[(\tilde{\mathbf{x}}_{k/k-1} - \tilde{\mathbf{x}}_{k/k})(\tilde{\mathbf{x}}_{k/k-1} - \tilde{\mathbf{x}}_{k/k})^{\mathrm{T}}] \qquad (19) \\ &\quad = E[\tilde{\mathbf{x}}_{k/k-1}\tilde{\mathbf{x}}_{k/k-1}^{\mathrm{T}} - \tilde{\mathbf{x}}_{k/k}\tilde{\mathbf{x}}_{k/k-1}^{\mathrm{T}} \\ &\qquad - \tilde{\mathbf{x}}_{k/k-1}\tilde{\mathbf{x}}_{k/k}^{\mathrm{T}} + \tilde{\mathbf{x}}_{k/k}\tilde{\mathbf{x}}_{k/k}^{\mathrm{T}}]. \qquad (20) \end{aligned}$$

Since

$$\tilde{\mathbf{x}}_{k/k} = \hat{\mathbf{x}}_{k/k} - \mathbf{x} = (\mathbf{I} - \mathbf{K}_k\mathbf{h}_k)\tilde{\mathbf{x}}_{k/k-1} + \mathbf{K}_k v_k, \tag{21}$$

$$E[\tilde{\mathbf{x}}_{k/k-1}\tilde{\mathbf{x}}_{k/k-1}^{\mathrm{T}} - \tilde{\mathbf{x}}_{k/k}\tilde{\mathbf{x}}_{k/k-1}^{\mathrm{T}} - \tilde{\mathbf{x}}_{k/k-1}\tilde{\mathbf{x}}_{k/k}^{\mathrm{T}} + \tilde{\mathbf{x}}_{k/k}\tilde{\mathbf{x}}_{k/k}^{\mathrm{T}}] \tag{22}$$

$$\begin{aligned} &= \mathbf{P}_{k/k-1} + \mathbf{P}_{k/k} - E[(\mathbf{I} - \mathbf{K}_k\mathbf{h}_k)\tilde{\mathbf{x}}_{k/k-1}\tilde{\mathbf{x}}_{k/k-1}^{\mathrm{T}} \\ &\quad + \mathbf{K}_k v_k\tilde{\mathbf{x}}_{k/k-1}^{\mathrm{T}} + \tilde{\mathbf{x}}_{k/k-1}\tilde{\mathbf{x}}_{k/k-1}^{\mathrm{T}} \\ &\quad \times(\mathbf{I} - \mathbf{K}_k\mathbf{h}_k)^{\mathrm{T}} + \tilde{\mathbf{x}}_{k/k-1}v_k\mathbf{K}_k^{\mathrm{T}}], \qquad (23) \\ &= \mathbf{P}_{k/k-1} + \mathbf{P}_{k/k} - 2\mathbf{P}_{k/k} = \mathbf{P}_{k/k-1} - \mathbf{P}_{k/k}. \qquad (24) \end{aligned}$$

Eq. (19) can be described in another form as

$$\begin{aligned} &E[(\hat{\mathbf{x}}_{k/k-1} - \hat{\mathbf{x}}_{k/k})(\hat{\mathbf{x}}_{k/k-1} - \hat{\mathbf{x}}_{k/k})^{\mathrm{T}}] \\ &\quad = E[\mathbf{K}_k(\mathbf{z}_k - \mathbf{h}_k\hat{\mathbf{x}}_{k/k-1})(\mathbf{z}_k - \mathbf{h}_k\hat{\mathbf{x}}_{k/k-1})^{\mathrm{T}}\mathbf{K}_k^{\mathrm{T}}], \qquad (25) \end{aligned}$$

where

$$\begin{aligned} \hat{\mathbf{x}}_{k/k-1} - \hat{\mathbf{x}}_{k/k} &= -\mathbf{K}_k(\mathbf{z}_k - \mathbf{h}_k\hat{\mathbf{x}}_{k/k-1}) = -\mathbf{K}_k\mathbf{v}_k \qquad (26) \\ &= E[\mathbf{K}_k\mathbf{v}_k\mathbf{v}_k^{\mathrm{T}}\mathbf{K}_k^{\mathrm{T}}]. \qquad (27) \end{aligned}$$

References

Blair, W. D. (1993). Fixed-gain two stage estimators for tracking maneuvering targets. *IEEE Transaction on Aerospace and Electronic Systems*, *29*, 1004–1014.

Bogler, P. L. (1987). Tracking a maneuvering target using input estimation. *IEEE Transaction on Aerospace and Electronic Systems*, *AES-23*, 298–310.

Chui, C. K., & Chen, G. (1991). *Kalman filtering* (2nd ed.). Berlin: Springer.

Harvey, A. C. (1992). *Time series models* (2nd ed.). Cambridge: MIT Press.

Kailath, T. (1968). An innovations approach to least squares estimation Part I: Linear filtering in additive white noise. *IEEE Transactions on Automatic Control*, *AC-13*, 646–660.

Kim, J. H., & Oh, J. H. (2000). A land vehicle tracking algorithm using stand-alone GPS. *Control Engineering Practice*, *8*, 1189–1196.

Leonhardt, D.A. (1997). Fine pitch packaging: Trends and technology. *Semicon West*.

Lui, D. S., Chao, Y. C., & Wang, C. H. (2004). Study of wire bonding looping formation in the electronic packaging process using the three-dimensional finite element method. *Finite Elements in Analysis and Design*, *40*, 263–286.

Mangoubi, R. S. (1998). *Robust estimation and failure detection*. London: Springer.

Ott, H. W. (1989). *Noise reduction techniques in electronic systems* (2nd ed.). New York: Wiley.

Rooney, D. T., Nager, D. P., Geiger, D., & Shanguan, D. (2005). Evaluation of wire bonding performance, process conditions, and metallurgical integrity of chip on board wire bonds. *Microelectronics Reliability*, *45*, 379–390.

Willsky, A., & Jones, H. (1976). A generalized likelihood-ratio approach to the detection and estimation of jumps in linear systems. *IEEE Transactions on Automatic Control*, *21*, 108–112.